Effect of Strain on Actomyosin Kinetics in Isometric Muscle Fibers

V. B. Siththanandan, J. L. Donnelly, and M. A. Ferenczi
Division of Biomedical Sciences, Imperial College London, London SW7 2AZ, United Kingdom

ABSTRACT Investigations were conducted into the biochemical and mechanical states of cross-bridges during isometric muscle contraction. Rapid length steps (3 or 6 nm hs^{-1}) were applied to rabbit psoas fibers, permeabilized and isometric, at either 12°C or 20°C. Fibers were activated by photolysis of P^3-1-(2-nitrophenyl)-ethyl ester of ATP infused into rigor fibers at saturating Ca^{2+}. Sarcomere length, tension, and phosphate release were recorded—the latter using the MDCC-PBP fluorescent probe. A reduction in strain, induced by a rapid release step, produced a short-lived acceleration of phosphate release. Rates of the phosphate transient and that of phases 3 and 4 of tension recovery were unaffected by step size but were elevated at higher temperatures. In contrast the amplitude of the phosphate transient was smaller at 20°C than 12°C. The presence of 0.5 or 1.0 mM added ADP during a release step reduced both the rate of tension recovery and the poststep isometric tension. A kinetic scheme is presented to simulate the observed data and to precisely determine the rate constants for the elementary steps of the ATPase cycle.

INTRODUCTION

The actomyosin interactions responsible for muscle contraction have been studied for many years, but the mechanical and biochemical events are yet to be fully integrated. Well-known work conducted in 1971 by Huxley and Simmons noted the complex force response of active isometric muscle to rapid release steps (1). These steps induce an elastic response consisting in a sudden drop in tension, followed by several phases of force recovery as the cross-bridges returned to a steady state. Smith and Sleep (2) recently produced a model to combine fast mechanical recovery with the phosphate-release step. They concluded that a fast, strain-dependent working stroke is likely to precede a slow phosphate-release step. Also Sleep et al. (3) suggested that a rapid, strain-dependent force-generating step is sandwiched between two strain-independent biochemical transitions (ATP hydrolysis and phosphate release). These studies are, however, based on mechanical measurements without direct biochemical data.

Since the development of *N*-(2-[1-maleimidyl]ethyl)-7-diethylamine-coumarin-3-carboxamide (MDCC)-PBP—a phosphate binding probe (PBP) with rapid and tight binding constants (4)—several studies have examined biochemical actomyosin kinetics in real time with millisecond time resolution. He et al. (5) outlined the scope of the probe in single fiber experiments and in later work used MDCC-PBP to examine the transition of initial ATPase rates to steady-state rates (6,7). Studies using cross-linked myofibrils and MDCC-PBP have suggested phosphate release may be the overall rate-limiting step in isometric contraction (8). One way to reconcile this finding with fiber work was to assume a very low duty cycle (<5%), whereby most cross-bridges were in weakly attached states and thus limited by phosphate release (8). Solution studies with the probe have also revealed information on the biochemical cycle (9) although, being in solution rather than a fiber, the results do not incorporate the effect of cross-bridge strain. Solution experiments also usually require a nonphysiological ionic strength of 20 mM or less (10). Notwithstanding such drawbacks, solution studies have relevance to muscle fibers. White et al. (9) found that when an equilibrated mixture of M·ATP and M·ADP·P_i was mixed with excess actin, actin rapidly bound M·ADP·P_i. The observed rate of phosphate release was biphasic. The fast phase was attributed to the immediate release of phosphate from A·M·ADP·P_i. The slow phase was due to M·ATP, which would first bind actin and then undergo nucleotide hydrolysis (the rate-limiting step when actin is saturating) before releasing phosphate. Experiments at higher temperatures showed that the rate of hydrolysis was enhanced, leading to a shift in the M·ATP/M·ADP·P_i ratio that favored the hydrolyzed state. As a result, upon introduction of actin, the amount of phosphate released in the fast phase was larger.

It is therefore opportune to examine the effects of strain perturbations on the biochemical transitions within muscle fibers. Such work may shed light on force-generating states in isometric contraction and provide direct evidence to integrate the phosphate-release step. Here work is presented that combines the use of P^3-1-(2-nitrophenyl)-ethyl ester of ATP (NPE) and MDCC-PBP to look at effects of rapid release steps on actomyosin kinetics in fibers during isometric contraction. The effects of added ADP are also examined as the presence of the nucleotide is likely to alter the initial distribution of cross-bridge states. A kinetic scheme, derived from other models in the literature (3,11), is used to interpret the results of rapid release experiments during isometric contraction of mammalian muscle fibers at 12°C and 20°C. The fit to the kinetic scheme is highly constrained as it needs to account for the time course of force development after

Submitted August 10, 2005, and accepted for publication February 9, 2006.

Address reprint requests to M. A. Ferenczi, Imperial College London, Sir Alexander Fleming Bldg., South Kensington, London SW7 2AZ, UK. E-mail: m.ferenczi@imperial.ac.uk.

0006-3495/06/05/3653/13 $2.00

doi: 10.1529/biophysj.105.072413

photolytic release of ATP, as well as during and subsequent to the quick length steps. In all the above phases the kinetic scheme is also constrained by the observed rate of phosphate release. The same kinetic scheme accounts for all parameters at 12°C and 20°C by assigning reasonable temperature dependence to relevant rate constants.

METHOD

Fiber preparation and experimental apparatus

Muscle fibers were harvested from New Zealand exbreeder rabbits (>5 kg) sacrificed by an intravenous overdose of sodium pentobarbital (100–200 $mg.kg^{-1}$), followed by dislocation of the spinal cord in accordance with Home Office Schedule 1 Protocol (UK). Psoas major muscle samples were taken, preserved, and stored as described in Thirlwell et al. (12). Fiber preparation and the experimental apparatus have also been described in detail elsewhere (7,13). Briefly, single fibers were dissected in a relaxing solution to a length of 4–5 mm and aluminum T-clips crimped onto each end. The points of attachment were fixed with a 0.4% glutaraldehyde solution while the fiber was in rigor. Presence of 20 mM 2,3-butanedione monoxime (Sigma, St. Louis, MO; B-0753) lowered rigor tension to limit damage. The fiber preparation was mounted on hooks and held in a temperature-controlled, rotating stage with five stainless steel and one quartz trough. One hook was connected to a tension transducer (Memscap AS, Skoppum, Norway, type 801, frequency response 1.6 kHz) and the other to a servo-motor capable of making longitudinal movements of up to 0.1 mm within 500 μs. To record sarcomere shortening during contraction, sarcomere length was monitored from the diffraction pattern formed by a 632.8-nm He-Ne laser (Lambda Photometrics, Herts, UK; LGK 7627) shone through the fiber and focused by a cylindrical lens onto a position sensitive photodiode.

Fluorescence measurements (lamp)

A Zeiss microscope with 40× water immersion objective (Zeiss, Jena, Germany; 40/0.75 W), modified to fit a photomultiplier tube (PMT) (Thorn, type 99224 QB) and tungsten lamp (12 V, 100 W), measured epifluorescence. Excitation was at 420 nm (interference filter, Ealing, Rocklin, CA; 35-3284 T-AVR, $\%T = 50.7$, fullwidth at half-maximum (FWHM) = 10 nm), and emission at 460 nm (interference filter, Glen Spectra, Stanmore, UK; DF10 0242 DTM, $\%T = 70$, FWHM = 10 nm). A dichroic mirror (reflecting at 350–425 nm, >450 nm $\%T = 95$) separated the filters.

Fluorescence measurements (laser)

In later experiments the fluorescence setup previously described was modified to increase the signal/noise ratio. The tungsten lamp used to provide the excitation light was replaced with a 4-mW, 440-nm laser diode module (Laser2000, PPM16(LD1504)G2). The laser was mounted in the same position as the lamp and epifluorescence was measured in the same manner. Due to the coherence and intensity of the laser light the following adjustments were made: first, the excitation filter was no longer required as the light was already at the correct wavelength (the same dichroic mirror and emission filter were used), and the voltage of the PMT amplifier was reduced from 500 to 300 V to prevent saturation. The modification resulted in a 2.5-fold reduction in the standard deviation of the baseline fluorescence signal.

Protocol

Once a fiber was mounted, the trough temperature was set to either 12°C or 20°C. Sarcomere length was set to 2.4 μm based on the fiber's diffraction pattern. The fiber was cleaned in a 1% (v/v) Triton X-100 relaxing solution for 30 min to remove membranous material. Fiber dimensions were measured under the 40× objective. Fiber width and depth were used to calculate cross-sectional area (CSA), assuming an elliptical cross section. Fiber length was taken as the distance between the areas of glutaraldehyde fixation (clearly visible under the objective). The servo-motor voltage was adjusted to impose a length step of the required amplitude, and hook movement was measured under the microscope (40× objective). For all experiments, incubation steps were the same (Table 1 summarizes the solutions used). Solutions for 12°C and 20°C were adjusted to take account of changes in the pKa values of the chemicals. Loading solutions of varying ADP concentrations were adjusted with K^+ propionate to maintain 150 mM ionic strength.

Each fiber was activated by immersion in prerigor solution for 3 min, followed by transfer to rigor solution containing a phosphate ''mop'' (14)—1 U ml^{-1} PNPase (bacterial purine nucleoside phosphorylase, Sigma, N-8264) and 0.5 mM 7-MEG (7-methylguanosine, Sigma, M-0627)—to remove free phosphate by sequestering it in the form 7-MEG-P_i. Free phosphate would otherwise bind MDCC-PBP and reduce its capacity. After 15 min the fiber was transferred into Ca^{2+} rigor solution (saturating calcium, 32 μM) for 7 min. Finally the fiber was infused for 15 min with a loading solution containing NPE-caged ATP (provided by M. Webb and G. Reid, NIMR, Mill Hill, London); MDCC-PBP (the fluorescent PBP; MDCC and unlabeled PBP provided by J. Corrie and M. Webb, NIMR), and the phosphate mop to reduce any phosphate contamination. As a precaution, the phosphate mop was allowed to work for around 2 h before the MDCC-PBP was added to the loading solution. In these experiments no ATP regeneration system was used; this allowed the concentrations of substrates to be accurately determined at any time point based on MDCC-PBP measurements. In ADP experiments the loading solution contained either 0.5 or 1 mM ADP (Sigma, A-6646, 97% pure). Before activation the fiber was transferred to a quartz trough filled with silicon oil (VWR, Lutterworth, UK; 200/10 cs) and the objective lowered. Contraction was initiated via a 347-nm, 80–100-mJ, 30-ns ruby laser pulse (frequency doubled from 694 nm and passed through a 340-nm band-pass filter, Ealing, $\%T = 85$), which liberates ~1.5 mM ATP from the NPE-caged ATP (approximate yield is 28%). Before the 340-nm band-pass filter, a beam-splitter tapped off 3.6% of main

TABLE 1 Solutions used in fiber experiments

	Relaxing	Prerigor	Rigor	Ca^{2+} rigor	Loading
TES	60	60	60	60	60
ATP	5	0.1	–	–	–
Free Mg^{2+}	5	5	5	5	5
K_2^+ EGTA	30	30	30	0.1	0.1
*Ca^{2+} EGTA	–	–	–	30	30
PNPase (U ml^{-1})	–	–	1	–	1
7-MEG	–	–	0.5	–	0.5
Glutathione	–	–	–	–	10
†NPE-caged ATP	–	–	–	–	5.5
‡ADP	–	–	–	–	0, 0.5, or 1
MDCC-PBP	–	–	–	–	1.5

Concentrations are in millimolar unless stated otherwise. All solutions were made up to 150 mM ionic strength using K^+ propionate, pH adjusted to 7.1 using 5 mM HCl and 5 mM KOH.

*Adjusted to give 32 μM free Ca^{2+}.

†NPE-caged ATP photolysis is ~28%.

‡ADP concentration varies depending on experiment.

TES, *N*-tris[hydroxymethyl]ethyl-2-aminoethanesulfonic acid; EGTA, 1,2-di (2aminoethoxy)ethane-*N*,*N*,*N*′,*N*′-tetra-acetic acid; PNPase, purine nucleoside phosphorylase; 7-MEG, 7-methylguanosine; NPE-caged ATP, P^3-1-(2-nitrophenyl)ethyl ester of ATP; MDCC-PBP, *N*-[2-(1-maleimidyl)ethyl]-7-(diethylamino)coumarin-3-carboxamide-phosphate binding protein (active concentration).

beam energy reaching the fiber. The 347-nm energy was recorded for each pulse, using a pyroelectric energy probe (Energy Max, Louisville, KY; J25 series) connected to an energy meter (Coherent, Santa Clara, CA; EPM1000). Glutathione, present in the loading solution, reduced damage from free radicals generated by the laser, although rarely would fibers be activated more than once.

Phosphate probe

The fluorescence signal was converted to MDCC-PBP-bound phosphate using Eq. 1, where ΔF is the change in fluorescence. MDCC-PBP has an activity of ~70% (determined from phosphate titrations). The remaining 30% does not bind phosphate. All references to probe concentration are active concentrations.

$$[\text{MDCC-PBP} \cdot P_i] = (\Delta F \times [\text{MDCC-PBP}]_{total})/\Delta F_{max}. \quad (1)$$

A transient drop in fluorescence was observed after the laser flash caused by a short-lived aci-nitro intermediate of caged ATP breakdown. Rate constants for aci-nitro decay are 46 s^{-1} at 12°C and 102 s^{-1} at 20°C (6). Fluorescence signals were corrected using an exponential with the appropriate rate constant and amplitude to match that of the data. The artifact, however, was small and did not affect the response to length steps as it subsided long before the length steps were imposed.

Many of the characteristics of MDCC-PBP within a fiber have been previously determined (5,6). The probe's binding rate constant, however, had only been established in solution via rapid stopped flow analysis (4). While the second order rate constant was found to be high, 1.36 × 10^8 $M^{-1}s^{-1}$ at 22°C, the validity of the rapid release step experiments here depends on a similarly large rate constant existing in studies with skinned muscle fibers. The response of the probe to sudden release of phosphate from NPE-caged phosphate (provided by G. Reid, NIMR) was determined within muscle fibers at 12°C. Fibers were prepared as described above. In the final loading solution, the fiber was infused with 1 μM MDCC-PBP and between 2.6 and 6.1 μM NPE-caged phosphate (pretreated with the phosphate mop to remove phosphate contamination). The probe concentration was kept low to approach first order kinetics. As a consequence, fluorescence changes were small and noisy. To improve the signal/noise ratio, experiments were performed on bundles of 3–4 fibers, thereby enlarging the amount of MDCC-PBP within the objective's field of view. The bundles were prepared with care to ensure all fibers ran parallel and that no fiber was enclosed in the center (which would limit diffusion and fluorescence emission). Fibers were flashed by the laser in the same manner as for ATP activation. After photolysis, calculation of the final free phosphate concentrations were based on calibration experiments which found the amount of NPE-caged phosphate converted to phosphate to be 57 ± 3% (n = 9) mean ± SE. The released phosphate was bound by MDCC-PBP, resulting in an increase in fluorescence. The rate of fluorescence increase was fitted with a single exponential and the rate constant determined (Fig. 1 *A*). No account was taken of the aci-nitro decay because after photolysis of caged phosphate, unlike caged nucleotides, the decay is very rapid and subsides within 100 μs (15). The maximum amount of phosphate released was limited to 3.5 μM. At concentrations above this the rate of binding was so rapid that it occurred almost completely within the laser flash artifact. The lowest concentration of phosphate released was 1.5 μM to ensure probe saturation. Determined binding rate constants were plotted individually against the amount of phosphate released (Fig. 1 *B*). These data were used to plot 95% confidence limits. As a result of using NPE-caged phosphate there was an inherent variation in the concentration of phosphate released, but the variation was small (±0.1 μM) and similar for all data points. Accordingly error bars for phosphate concentration are omitted from Fig. 1 *B*. The gradient of the plot gives a second order binding rate constant for the probe of 7.70 × 10^7 $M^{-1}s^{-1}$ at 12°C. This value is consistent with that found by Brune et al. (4) at 22°C in solution.

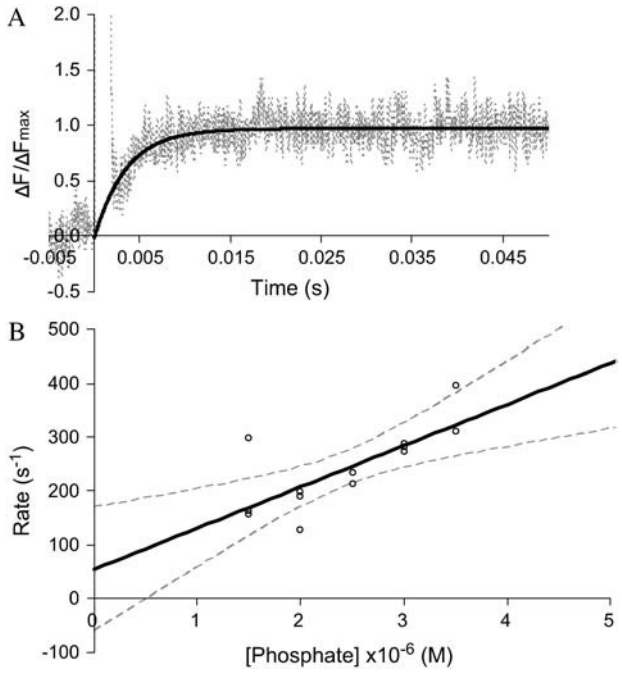

FIGURE 1 MDCC-PBP assay for phosphate release. (*A*) Normalized fluorescence signal from the photolytic release of 3.0 μM phosphate (single experiment) in a fiber bundle (4 fibers, Ca^{2+} free rigor, 12°C, CSA 2.87 × 10^{-8} m^2) infused with 1 μM MDCC-PBP. Laser flash, at time 0, causes an artifact lasting ~2 ms. Preflash fluorescence signal is 0, and maximum fluorescence change is 1. A single exponential (*black line*), fitted through zero fluorescence at time 0, is fitted to the fluorescence change (from 2 to 100 ms); rate constant is 281 s^{-1}. The fiber bundle was flashed while immersed in silicone oil. Data smoothed with a 25-point Savitsky-Golay algorithm. Data sampling rate 32 kHz. (*B*) Phosphate binding rates of MDCC-PBP (as determined in *A*) plotted against concentration of phosphate released. Experiments were on three separate bundles of fibers (3–4 fibers per bundle), average CSA 2.39 × 10^{-8} m^2. Linear fit (*black line*) has a slope of 7.7 × 10^7 $M^{-1}s^{-1}$. Also shown are 95% confidence limits (*dashed gray lines*).

Data collection

Data for tension, fluorescence, and sarcomere length were recorded at 6.4 kHz using a National Instruments (Austin, TX) A-D card installed on a PC with associated TestPoint program. Additionally, high time resolution data (20 MHz) were recorded on an oscilloscope (Tektronix 5223) for a 5-ms period during and immediately after the step. These data were transferred onto a PC via a CEC (Middleboro, MA) IEEE card and TestPoint program. No signal filters were applied before data acquisition, but for analysis a first order, 25-point Savitsky-Golay smoothing algorithm was applied to the fluorescence traces (using MatLab 6.5.1; MathWorks, Natick, MA). This was preferred over a moving average to prevent loss of subtle transients, especially in the fluorescence signal. Data were analyzed using MS Excel. Unless stated, all errors are mean ± 1 SE.

RESULTS

Typical records for tension, sarcomere length, and phosphate release are shown in Fig. 2, *A–C*. The records are averages of single experiments from six separate fibers. Contractions

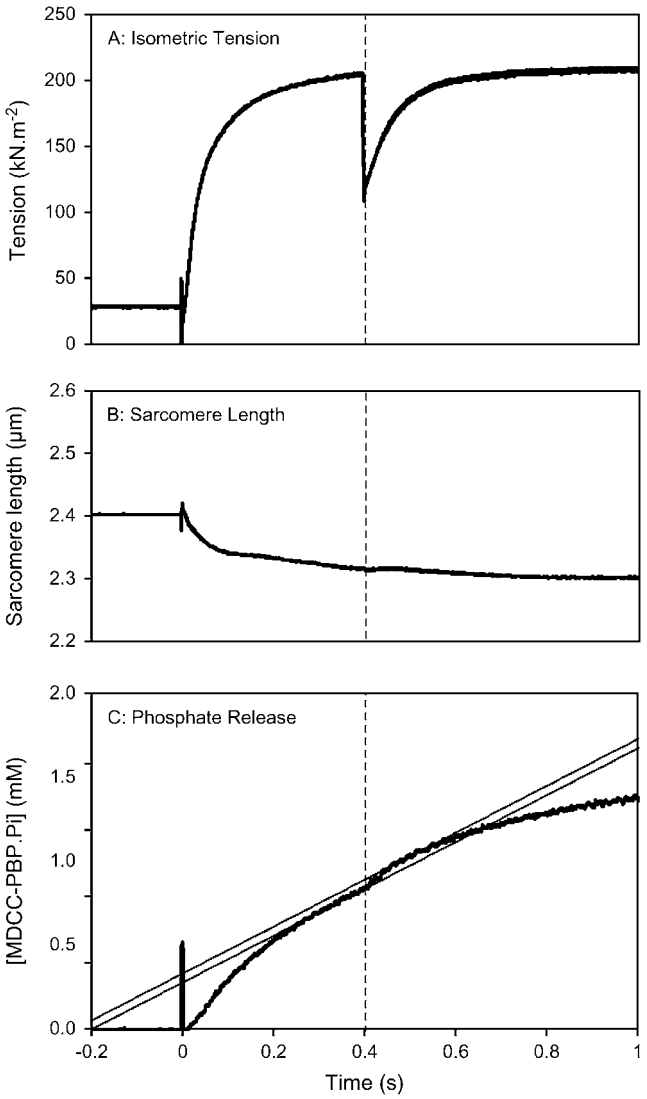

FIGURE 2 Time courses of force, sarcomere length, and phosphate release. Typical experimental records averaged from single fiber experiments. (*A*) Development of isometric tension ($n = 6$); (*B*) sarcomere length ($n = 4$); and (*C*) phosphate release ($n = 4$) calculated from the MDCC-PBP fluorescence signal. Experiments were at 12°C, average CSA 3.01×10^{-9} m^2. Fibers were activated from Ca^{2+} rigor (32 μM free Ca^{2+}), using a laser pulse to release ATP from NPE-caged ATP (5.5 mM). Released phosphate bound to 1.5 mM MDCC-PBP present in the fiber. Fibers were placed in silicone oil during activation to ensure that the fluorescence signal emanated only from within the fiber and to prevent diffusion of solutes out of the fiber. Laser flash was at time 0, and the release step (0.5% of fiber length) was at 0.4 s (*vertical dashed line* in all records). Linear fits in panel *C* to the pre- (0.3–0.4 s) and post- (0.45–0.55 s) step data are shown by the thin lines. Data smoothed with a 25-point Savitsky-Golay algorithm. Data sampling rate, 64 kHz.

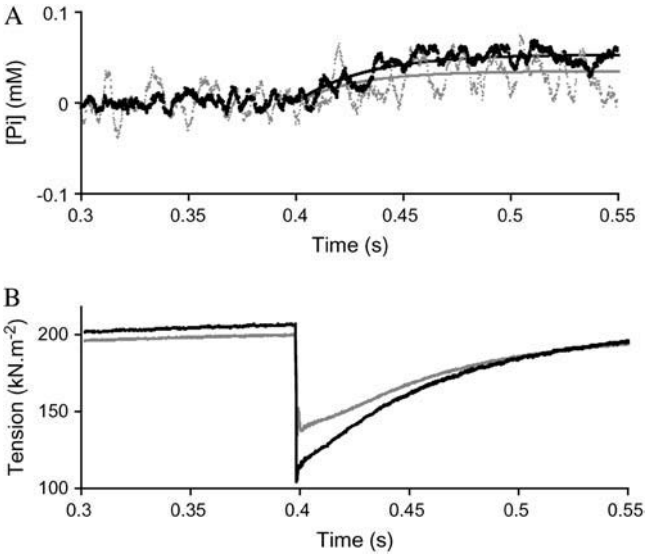

FIGURE 3 Response to rapid length steps at 12°C. (*A*) Phosphate release, calculated from the MDCC-PBP fluorescence signal by subtraction of the steady-state signal (see text). Averages from single experiments, 0.3%*L* step (*gray*, $n = 6$) and 0.5%*L* step (*black*, $n = 4$). Single exponentials, fitted through zero [P_i] at time 0.4 s, are fitted to the transients; rate constant are 35 ± 3 s^{-1} ($n = 6$, 0.3%*L*, *gray line*) and 32 ± 5 s^{-1} ($n = 4$, 0.5%*L*, *black line*). (*B*) Tension recovery records, averaged from single experiments, after rapid release steps of 0.3%*L* (*gray*, $n = 6$) and 0.5%*L* (*black*, $n = 6$). In both panels *A* and *B*, data for 0.5%*L* release steps are the same as that shown in Fig. 2. Data for 0.3%*L* release steps were obtained under the same conditions, average CSA 5.11×10^{-9} m^2.

were at 12°C, and length steps were 0.5% of the fiber length (*L*). A 0.5% *L* step equates to a movement of ~6 nm.hs^{-1} of the isometric fiber, determined from the motor hook displacement during the step. The laser pulse occurred at 0 s, releasing ATP and creating a flash artifact lasting ~4 ms (seen in all records). After a transient drop in tension of 5–10 kN m^{-2}, rapid tension development followed until an isometric level was reached, 213 ± 4 kN m^{-2} ($n = 6$) (Fig. 2 *A*). During the plateau, at 0.4 s, the length step was imposed. The resultant drop in tension was followed by a period of complex tension recovery until prestep tension was once again attained (see Fig. 3 *B*).

During the initial tension rise there was a fast phase of shortening as reported by the sarcomere length measurements (Fig. 2 *B*). Shortening of the sarcomeres was <0.1 μm and largely over within 100 ms. Thereafter sarcomere length decreased slowly. Some additional sarcomere shortening is also seen at the point of the length step. Despite air conditioning in the laboratory, days with high ambient humidity caused condensation to rapidly develop on the quartz window. This often prevented the sarcomere length from being monitored. Overall, sarcomere length was successfully monitored in 60% of experiments.

The phosphate-release record (Fig. 2 *C*), derived from the fluorescence signal, shows a fast initial rate during tension development. The rate then slows, and by 0.2 s has reached a steady rate of 9.2 ± 1.0 s^{-1} ($n = 4$). The step perturbation caused a transient in the rate of phosphate release, albeit short lived, before returning to the steady rate. The amount of MDCC-PBP that could be infused into a fiber was restricted; therefore saturation occurred early, and after ~0.6 s the sig-

nal began to plateau. Linear fits were made to the steady rates before and after the step (prestep is fitted from 0.3 to 0.4 s; poststep is fitted from 0.45 to 0.55 s). The pre- and poststep gradients were similar and averaged for ease of analysis. Calculations were made using MS Excel Solver. Fig. 2 *C* shows the fits as thin solid lines.

Fig. 3 shows analysis and comparison of phosphate and tension records for 0.3%*L* and 0.5%*L* step sizes at 12°C. The phosphate-release transient (Fig. 3 *A*: *black* is the 0.5%*L* step; *gray* is the 0.3%*L* step) was isolated by subtraction of the steady rate from the phosphate record. A single exponential—fitted through zero phosphate concentration at 0.4 s—was fitted to each transient, providing a rate constant and amplitude. As step size increased from 0.3 to 0.5%*L*, the rate constant varied little ($35 \pm 3\ s^{-1}$, $n = 6$, for 0.3%*L* and $32 \pm 5\ s^{-1}$, $n = 4$, for 0.5%*L*). The amplitude, which represents the extra amount of phosphate released due to the step, rises from $31 \pm 9\ \mu M$ ($n = 6$) for 0.3%*L* steps, to $52 \pm 9\ \mu M$ ($n = 4$) for 0.5%*L* steps. On the same expanded time axis as phosphate release are the corresponding tension records (Fig. 3 *B*). The early phases of tension recovery were not well resolved. The limited speed of the motor (length steps were completed in 500 μs) allows for truncation of phase 1 by phase 2 (1). Thus our analysis is restricted to phases 3 and 4. The apparent presence of phase 2 in Fig. 3 *B*, which is more evident for the larger step, is an artifact principally due to the undamped response of the tension transducer (16), as discussed later. The effect for the larger step is about twice that of the 3 $nm.hs^{-1}$ step. Single exponentials were fitted to the combined phases 3 and 4 of force recovery (not plotted) to determine the rates. The rate of force recovery was $13 \pm 1\ s^{-1}$ ($n = 6$) for a 0.3%*L* release and $14 \pm 1\ s^{-1}$ ($n = 6$) for 0.5%*L*.

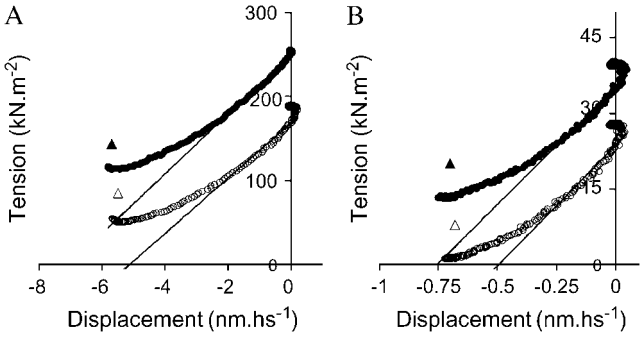

FIGURE 4 Muscle fiber stiffness. (*A*) Instant length-tension relationships during length steps of 0.5%*L* in active fibers, 0.4 s after activations, at 12°C (*open circles*) and 20°C (*solid circles*). Triangles denote the final tension after the subsidence of inertial artifacts within the tension response (see text). Data sampled every 5 μs during step. Linear fits are made as described in text. Slope of lines are 39 ± 2 MN m^{-2} ($n = 5$) at 12°C, and 43 ± 4 MN m^{-2} ($n = 4$) at 20°C. (*B*) Same as in panel *A*, but fibers are in Ca^{2+} rigor and steps are 0.1%*L*. Slope of lines are 57 ± 4 MN m^{-2} ($n = 3$) 12°C, and 56 ± 1 MN m^{-2} ($n = 3$) at 20°C.

It was possible to make an assessment of fiber stiffness during the phosphate assay experiments by simultaneously collecting high time resolution data of motor movement and tension over a 5-ms period encompassing the step. Fig. 4 *A* shows the motor displacement ($nm.hs^{-1}$) against the change in force due to the drop in strain for 0.5%*L* steps at 12°C and 20°C. Linear fits were made to the data, and fiber stiffness was determined from the gradient multiplied by the half-sarcomere length (1.2 μm). In all stiffness calculations the data incorporated by the linear fits, as shown in Fig. 4 *A*, were 70% of the total tension change resulting from the step, starting from the isometric tension. The 70% cutoff point was chosen to encompass the highest number of data points early in the step. The stiffness graphs would be linear if they were reporting a purely elastic T1 response. There are, however, several experimental factors influencing the tension response to a length step and the measurement of instantaneous stiffness (16). Apart from the speed of the length step, which is critical when fast force recovery processes occur in the cross-bridges (phase 2), the transducer response, fiber inertia, and viscosity of the fluid bathing the fiber all contribute to the time course of the force response. The force transducer used was undamped, resulting in an overshoot in the force responses. To appreciate the magnitude of these effects, plotted on Fig. 4 are the tension values after such artifacts have subsided. These points lie above the fitted lines, showing the active stiffness measurements are overestimated by ~45%. However, using our estimates of stiffness, the effect of temperature is small; the slopes of the lines in Fig. 4 *A* differ by <10%.

Fiber stiffness in rigor was also assessed by the same method and at 12°C and 20°C (Fig. 4 *B*). As stiffness is higher in rigor, release steps were only 0.1% of fiber length to prevent the fibers going slack. Temperature has little effect on rigor stiffness. At 12°C and 20°C measured stiffness differed by <2%. In rigor also the linear fits overestimate stiffness. The overestimate is ~49%, which is greater than in the active measurements because of the lack of phase 2 recovery in rigor.

These data, however, only reveal the active stiffness at 0.4 s into contraction. In separate experiments, without the MDCC-PBP probe present, multiple length steps were performed on fibers at 12°C in rigor and when activated to see how stiffness changed during contraction. During each contraction four consecutive rapid length steps of 0.3%*L* each were performed at either 100, 200, 300, and 400 ms ($n = 7$) or at 25, 125, 225, and 325 ms ($n = 5$). In rigor, similarly, the same step protocol was used but with step sizes of 0.1%*L*. Each length step was separated by 100 ms to allow the cross-bridges to reequilibrate. In the absence of MDCC-PBP to remove phosphate, isometric tensions (181 ± 10 kN m^{-2}, $n = 12$) were 13% lower then in its presence at 12°C. The data for the time course of stiffness changes were used qualitatively in the kinetic model (see Kinetic model section and Fig. 9 *B*).

TABLE 2 Measured mechanical and biochemical parameters during rapid length steps

Temperature(°C)	12		20	
Step size				
% Fiber length (%*L*)	0.30	0.50	0.25	0.50
Per half-sarcomere (nm hs^{-1})	−3.6 ± 0.1 ($n = 5$)	−5.5 ± 0.2 ($n = 5$)	−2.9 ± 0.3 ($n = 5$)	−5.8 ± 0.2 ($n = 4$)
Isometric tension(kN m^{-2})	203 ± 19 ($n = 6$)	213 ± 4 ($n = 6$)	282 ± 25 ($n = 5$)	250 ± 13 ($n = 5$)
Tension recovery (phase 3/4) rate(s^{-1})	13 ± 1 ($n = 6$)	14 ± 1 ($n = 6$)	30 ± 4 ($n = 5$)	23 ± 4 ($n = 5$)
Steady rate of P_i release(s^{-1})	7.9 ± 1.3 ($n = 6$)	9.2 ± 1.0 ($n = 4$)	8.5 ± 2.0 ($n = 4$)	9.0 ± 1.0 ($n = 5$)
Transient P_i release rate(s^{-1})	35 ± 3 ($n = 6$)	32 ± 5 ($n = 4$)	83 ± 34 ($n = 4$)	88 ± 25 ($n = 5$)
Transient amplitude(μM)	31 ± 9 ($n = 6$)	52 ± 9 ($n = 4$)	10 ± 2 ($n = 4$)	30 ± 5 ($n = 5$)

Calculations of phosphate release assume a myosin head concentration of 0.15 mM. Tension recovery rate was determined by fitting a single exponential to phases 3 and 4 of recovery. Errors are mean ± 1 SE.

Effect of step size and temperature

Table 2 summarizes the results for release steps performed at both 12°C and 20°C. At higher temperatures maximum isometric forces were, overall, 28% greater. The Q_{10} values of tension recovery and phosphate transient rates were 2.5 and 3.2, respectively. There was, however, no substantial increase in the steady rate of phosphate release. Unlike temperature, step size did not influence either tension recovery or phosphate transient rates. The amount of phosphate released due to the step is of particular note. Larger steps caused more phosphate to be released than the smaller step at the same temperature (see transient amplitude values in Table 2). At 20°C, however, both the 0.3%*L* and 0.5%*L* steps released less phosphate than the same sized steps at 12°C.

Effect of added ADP

The same 0.5%*L* release experiments were repeated at 12°C but with varying concentrations of added ADP. Fig. 5 shows the normalized tension records for contractions with 0.0, 0.5, and 1.0 mM added ADP. Normalization was performed by taking the maximum isometric tension as 1 and the resting tension as 0 (all rigor tensions were similar at around 20 kN m^{-2} with no length adjustment). As ADP concentration is increased there is a delay before force production commences, and the rate of initial force generation is diminished—half-maximum tensions are reached at 50, 82, and 100 ms for 0.0, 0.5, and 1.0 mM added ADP, respectively. In the presence of added ADP the transient tension drop preceding initial tension development is absent (Fig. 6). Fig. 7 summarizes the alterations in the transient kinetics caused by added ADP compared to equivalent results where no ADP was added. Prestep isometric tensions remain fairly constant for 0.5 and 1.0 mM ADP at ~215 kN m^{-2}; marginally higher than with no added ADP. The rate of tension redevelopment after the step reduces from 14 ± 1 s^{-1} ($n = 6$) without added ADP to 10 ± 1 s^{-1} ($n = 4$) with 0.5 mM and 9 ± 1 s^{-1} ($n = 3$) with 1.0 mM. When no ADP is added the isometric tension de-

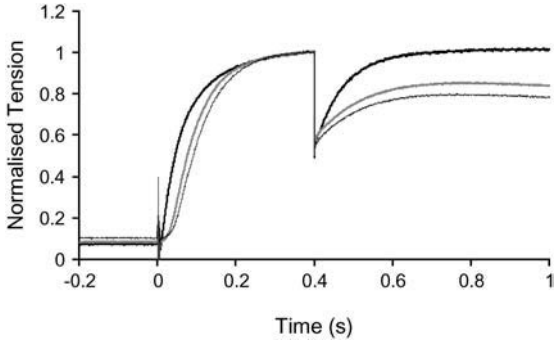

FIGURE 5 Effect of ADP on tension development. Tension records, averaged from single fiber experiments, were normalized between resting and isometric tension for contractions in absence of added ADP (*thick black line*, average CSA 3.01×10^{-9} m^2, $n = 6$), or in the presence of 0.5 mM added ADP (*thick gray line*, average CSA 6.36×10^{-9} m^2, $n = 4$) or 1.0 mM added ADP (*thin black line*, average CSA 5.01×10^{-9} m^2, $n = 3$). In all experiments fibers were activated from Ca^{2+} rigor at 12°C by photolytic release of ATP. A 0.5%*L* step was performed at 0.4 s. The rate of tension development and the poststep isometric tension are visibly reduced by the presence of ADP. Data sampling rate, 64,000 Hz.

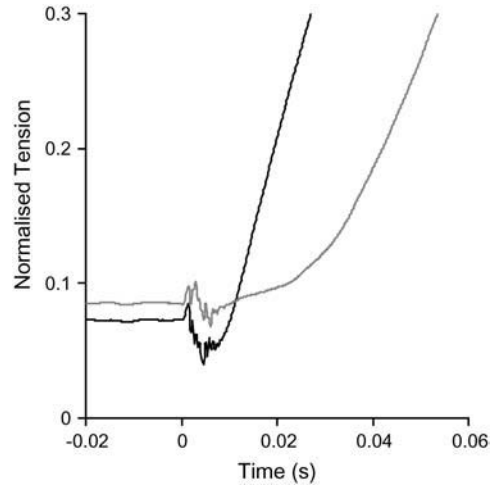

FIGURE 6 Force development after photolytic release of ATP. Normalized tension records in the absence of added ADP (*thick black line*) or in the presence of 0.5 mM added ADP (*thick gray line*), as shown in Fig. 5 but on expanded axis. When no ADP is added there is an initial drop in tension associated with cross-bridge detachment. This is less evident with 0.5 mM added ADP. The noise at the very start of contraction is an artifact resulting from the laser pulse.

veloped after a step returns to, or very close to, the prestep level. As the amount of added ADP is increased the recovered tension (in relation to maximum tension) drops to 86% at 0.5 mM and 77% at 1.0 mM (also see Fig. 5). Increases in the fiber stiffness are seen with added ADP; the estimated stiffness increases ~22% from 0.0 to 0.5 mM added ADP. Student's *t*-test analysis shows that, compared to the control, changes in the rates of tension recovery, the reduction in poststep isometric tensions and the increases in stiffness are all significantly different ($p \leq 0.05$). Other changes in kinetic parameters, such as phosphate release, were not significantly different. The steady rate of phosphate release was slightly lower in the presence of ADP, although at 0.5 and 1.0 mM the rates are similar, and the phosphate transient rate varied between $32 \pm 5\ s^{-1}$ ($n = 4$) at 0.0 mM, to $31 \pm 8\ s^{-1}$ ($n = 3$) at 0.5 mM, and $18 \pm 12\ s^{-1}$ ($n = 3$) at 1.0 mM. The amount of phosphate liberated by the step is also relatively unchanged in the presence of increased ADP concentrations, remaining between 50 and 60 μM.

Kinetic model

The experimental tension and phosphate-release records were modeled based on the actomyosin pathway shown in Scheme 1. In the model, tension was relative and phosphate release was in millimolars. Experimentally, no ATP regenerating system was used, so the model allowed nucleotide concentrations to vary. The rate of ATP binding and A·M. dissociation (k_1) was rapid, although at the start of contraction, the rate was limited by ATP release from NPE-caged ATP. Effects of increasing temperature from 12°C to 20°C were mainly accounted for in the hydrolysis step (Q_{10} of 5), which is highly temperature sensitive (3). The rate of ATP hydrolysis at 20°C was $200\ s^{-1}$, compared to literature values of $100\ s^{-1}$ (3) and $225\ s^{-1}$ (17). Once M·ADP·P_i reattached, the model assumed A·M·′ADP·P_i to generate force. A·M·′ADP·P_i and a post-phosphate-release state (A·M·′ADP) were required to generate force to satisfactorily describe the data. As shown in Table 3, the model assigns a relative force of 1 to A·M·′ADP at both 12°C and 20°C. But the relative force of A·M·′ADP·P_i is 2 at 12°C, and 3 at 20°C. In the model, A·M·′ADP·P_i holds more force than A·M·′ADP because the force assigned to a cross-bridge state was the average force for that particular cross-bridge population, whereas in reality, it is envisaged that the force held by an individual cross-bridge varies with the cross-bridge's displacement. Smaller cross-bridge displacements are considered to promote the transition of A·M·′ADP·P_i into A·M·′ADP, and the axial distribution of the A·M·′ADP cross-bridge population is assumed to be at a smaller average displacement than A·M·′ADP·P_i. The model does not explicitly incorporate cross-bridge displacement, so instead a lower force is assigned to A·M·′ADP to account for the smaller average displacement of the cross-bridges (Table 3). Other values for the force ratio of A·M·′ADP·P_i and A·M·′ADP produced poorer fits to the data.

Fiber elasticity was included when calculating the rate of force development, as in the model used in West et al. (11). For calculations: filament sliding velocity was determined from the force-velocity curve in Table 3, where calculated force per cross-bridge is the total calculated force divided by the sum of the A·M·′ADP·P_i and A·M·′ADP force-generating cross-bridges. The velocity was multiplied by the normalized fiber relative force per muscle length (ML) to give the rate of change of force. The rate constant for ADP release (k_5) was strain dependent. The rate constant was linked to tension; so that at isometric tension (at 12°C) $k_5 = 11\ s^{-1}$, and at zero tension $k_5 = 2915\ s^{-1}$ (shown as xk_5 in Table 3). Length steps were simulated by an immediate reduction in the modeled tension to match the drop in the experimental record. The size of the drop is shown as T_{drop} in Table 3. The actomyosin cycle (Scheme 1) is likely to have more than one strain-dependent step. The other main strain-dependent transition would be a nonforce to force generation isomerization of A·M·′ADP·P_i. Adding A·M·′ADP·P_i strain dependence would bring another level of complexity to the model and require the introduction of cross-bridge displacement dependence. This was not necessary to effectively model the release step data, though the rate constant for phosphate release (k_4) is twice the measured value for the phosphate-release rate. For this model to satisfactorily fit the phosphate record with strain dependence assigned only to ADP release and not to a prephosphate-release state, the k_4 rate constant was required to be faster than the observed rate. Other models (2,3), which used phosphate-release rates determined in solution (9), were not constrained by biochemical data. Due to the effectively irreversible binding of P_i to MDCC-PBP, the rate of phosphate binding (r_4) could

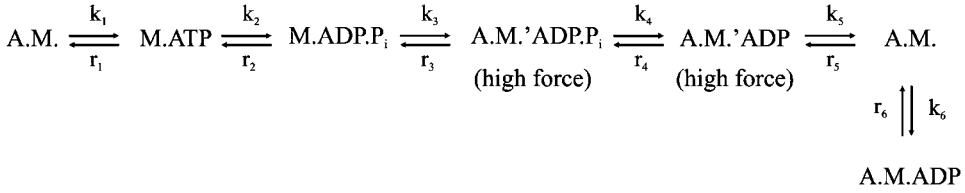

(Scheme 1)

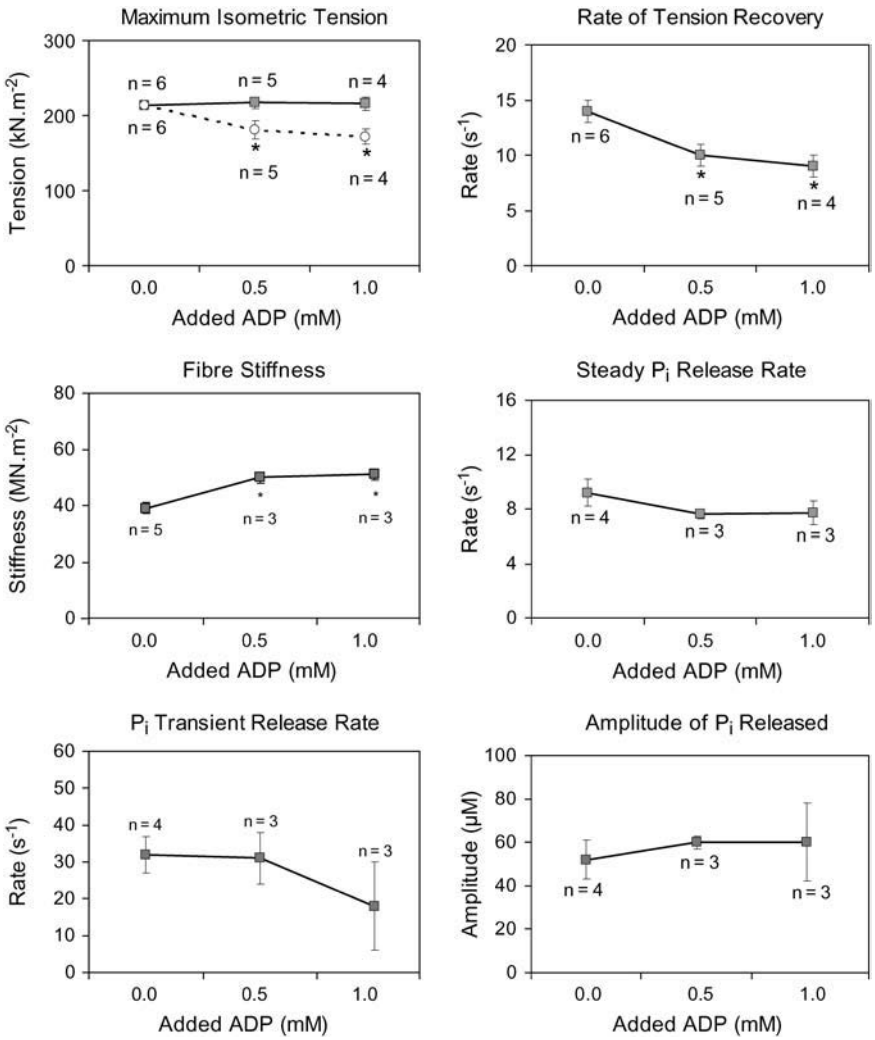

FIGURE 7 Effect of ADP on the observed mechanical and biochemical kinetics of contracting muscle fibers. Data are from averages of single fiber experiments. Contractions were at 12°C and a 0.5%*L* step was imposed 0.4 s after activation. The control (no added ADP) is the same data as shown in Fig. 1 and presented in Table 2. Plot of maximum isometric tension shows isometric tension before the step (*solid line* with *filled squares*) and after the step (*broken line* with *open circles*). Rate of tension recovery refers to phases 3 and 4 after the length step. Amplitude of phosphate released refers to the amount of extra phosphate released due to the step, as shown in Fig. 3 *A*. * indicates significant difference ($p \leq 0.05$, Student's *t*-Test) compared to control. All error bars are mean ± 1 SE.

not be measured from our data, and the assigned value had no effect on the simulations.

In the model the A·M·ADP state was assumed to form reversibly by ADP binding to rigor A·M. cross-bridges was non-force generating and strain independent. It was external to the cycle, so was not formed by ATP hydrolysis. The presence of NPE-caged ATP (photolysis is ~28%), which behaves as a competitive inhibitor of ATP (18), was accounted for by populating the A·M·ADP state (though NPE-caged ATP actually bound A·M. to form A·M.cagedATP, it is an A·M·ADP-like complex, and in Figs. 9 *B* and 10 *B* the A·M.cagedATP state is included with the A·M·ADP states). NPE-caged ATP could not bind A·M. to form an A·M·′ ADP-like state. In Table 3, k_6 and r_6 refer to the formation of A·M·ADP, and k_{6cage} and r_{6cage} refer to A·M.cagedATP. The time course of the fraction of attached cross-bridges was a quantity predicted by the model. During isometric contraction the calculated fraction of attachments did not remain constant as the model accounted for the absence of an ATP regeneration system in the experimental protocol and allowed the ATP/ADP ratio to vary. Experimental data were collected for the time course of changes in fiber stiffness. However, compliance within the filaments may be as high as cross-bridge compliance (19). The elasticity residing in the filaments causes an underestimate in the number of attached cross-bridges calculated from stiffness measurements. Due to this uncertainty and to that associated with the experimental measure of stiffness, stiffness data were not used to calculate the fraction of attached cross-bridges. Although the number of attached cross-bridges cannot be determined from our stiffness data, the time course of the experimental stiffness changes is in line with that expected for cross-bridge attachments: after scaling to rigor stiffness, the predicted time course of attached cross-bridges matches the stiffness observations well (*open circles*, Fig. 9 *B*).

The kinetic scheme was used to establish two sets of rate constants, one at 12°C and the other at 20°C. Fig. 8, *A–C*, shows the modeled and experimental data for phosphate release and tension during 0.3%*L* release steps at 12°C. All the rate constants are shown in Table 3. The free energy change

TABLE 3 Parameters used to calculate the time courses of changes in actomyosin states according to Scheme 1

Temperature (°C)	12	20
k_1 ($M^{-1}s^{-1}$)	1.0×10^6	2.0×10^6
r_1 (s^{-1})	**75**	**75**
k_2 (s^{-1})	50	200
r_2 (s^{-1})	25	150
k_3 (s^{-1})	**180**	**202**
r_3 (s^{-1})	**64**	**193**
k_4 (s^{-1})	76	176
r_4 ($M^{-1}s^{-1}$)	2.0×10^5	2.0×10^5
k_5 (s^{-1})	**11**	**12**
r_5 ($M^{-1}s^{-1}$)	$\mathbf{10 \times 10^3}$	$\mathbf{23 \times 10^3}$
k_6 ($M^{-1}s^{-1}$)	$\mathbf{80 \times 10^3}$	$\mathbf{80 \times 10^3}$
r_6 (s^{-1})	**40**	**40**
k_{6cage} ($M^{-1}s^{-1}$)	20×10^3	20×10^3
r_{6cage} (s^{-1})	40	40
xk_5 (s^{-1})	**2915**	**3840**
T_{drop}	0.3 (for 0.3%L step) 0.5 (for 0.5%L step)	0.5 (for 0.5%L step)
Velocity of shortening (ML.s^{-1})	$(0.51 - (0.51.F))/(F + 0.42)$	$(0.51 - (0.51.F))/(F + 0.085)$
Relative isometric fiber stiffness (F.ML^{-1})	18	18
Rate of ATP release from cage (s^{-1})	46	102
A·M·′ADP·P_i (relative force)	**2**	**3**
A·M·′ADP (relative force)	1	1

Rate constants in bold were fitted values; other values were largely obtained from the literature. k_{6cage}/r_{6cage} relate to the formation of A·M.caged.ATP (equivalent to A·M·ADP in Scheme 1; see text), giving a K_i of 2 mM (18). xk_5 is the maximum rate of ADP release from A·M·′ADP at zero tension. T_{drop} is the relative drop in force due to the step, at 12°C the values are for 0.3 and 0.5%L steps, respectively. Velocity of shortening was calculated from the force-velocity curve used in He et al. (7) at 12°C (V_{max} 1.25 ML s^{-1}). At 20°C the equation is altered to give a relative V_{max} of 6.25 ML s^{-1} (18). F is relative force; ML is muscle length. Relative fiber stiffness (at 0.4 s after activation) was obtained by normalization of experimental stiffness data (ratio of relative tension/step size in ML). A·M·′ADP·P_i includes force and nonforce isoforms, so the force at 12°C and 20°C is the average cross-bridge force of the whole population (see text).

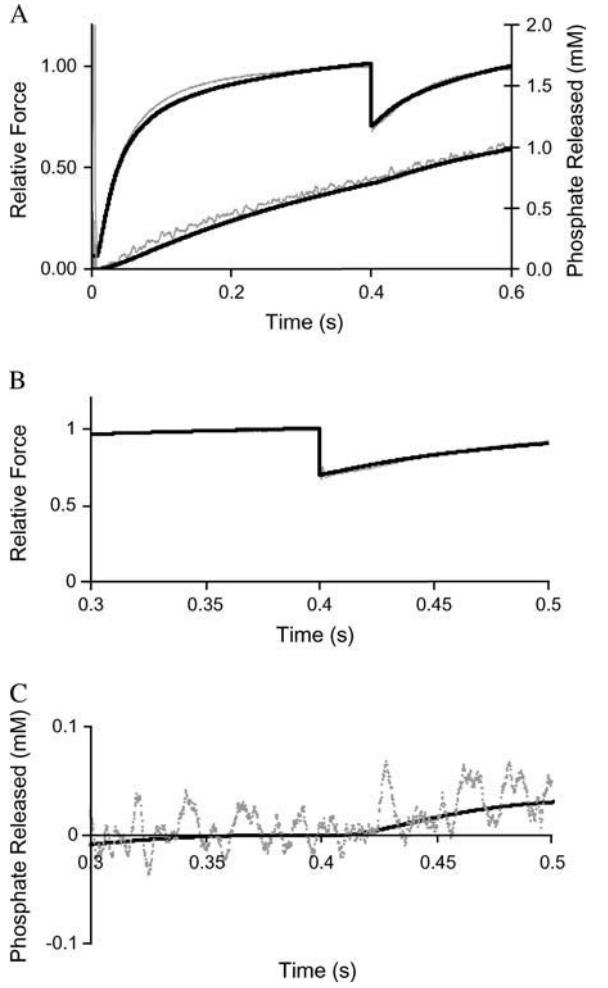

FIGURE 8 Comparison of observed data and model calculations using Scheme 1 and parameters listed in Table 3. (*A*) Experimental (*gray*) and calculated (*black*) records during isometric contraction with a 0.3%L step at 12°C. Relative tension is on the left-hand y axis, and phosphate release (in millimolar) is on the right-hand y axis. (*B*) Tension record shown in panel *A*, but on an expanded time axis encompassing the step and period of recovery. (*C*) Isolated phosphate transient resulting from the step (isolated using the same method as described in text for experimental data and shown in Fig. 3 *A*).

of the overall cycle was calculated. Variable substrate concentrations were taken as 1 mM ATP, 0.5 mM ADP, 10 μM phosphate (due to MDCC-PBP). The free energy at both temperatures was ~ -32 kJ mol^{-1}. The calculated free energy of ATP hydrolysis was -34 kJ mol^{-1} (20). Simulations were started with the release of ATP at a rate matching the rate of photolysis. Simulations were run in MatLab using time intervals of 12 μs. Eight rate constants were fitted using the fminsearch function of MatLab; these are shown in bold in Table 3. The total myosin head concentration was 0.15 mM.

DISCUSSION

Isometric contraction

Fibers were activated from rigor at saturating Ca^{2+}. In the model, before ATP release cross-bridges were either in the A·M. state (21) or had caged ATP bound (70% of heads, approximated from the k_{6cage} and r_{6cage} values in Table 3). The photolytic release of ATP (46 s^{-1} at 12°C or 102 s^{-1} at 20°C) caused rapid ATP binding and actomyosin dissociation. Cross-bridge cycling followed and tension developed rapidly. Once tension was isometric, within 0.3 s after activation the increased strain caused the ADP release step (k_5 in Scheme 1) to become rate limiting (22). The force plateau, however, is not a certain indicator of a true steady state as the ATPase rate continues to fall and ADP accumulates (11). A steady-state ATPase rate is likely to require tens of seconds to develop and to require an ATP-regenerating system (22). Here, experiments show the average steady phosphate-release rate before and after the step was 8.6 s^{-1} at 12°C,

in agreement with values published by He et al. (7) under similar conditions. At 20°C, however, the rate does not increase, because of the absence of an ATP backup system. At 20°C the more rapid buildup of ADP results in lower than expected ATPase rates.

In Fig. 9 *A* the modeled and observed data are shown for the first 0.3 s of contraction at 12°C. The figure shows the effect of incorporating fiber elasticity against which tension develops. Simulations reveal this has a notable influence on the rate of tension development and phosphate release. When the elasticity is removed from the model, the tension rise is even faster (*dotted black line* in Fig. 9 *A*). Little effect is seen on the rate of phosphate release in the first 50 ms, but thereafter the rate slows more rapidly than when elasticity is present (*dotted gray line* in Fig. 9 *A*). This is because elasticity allows shortening, during which phosphate release is accelerated. Fig. 9 *B* shows the time course of relative changes in experimental fiber stiffness, the calculated proportion of attached states, and the distribution of actomyosin states (Scheme 1) during this initial phase of contraction with elasticity present.

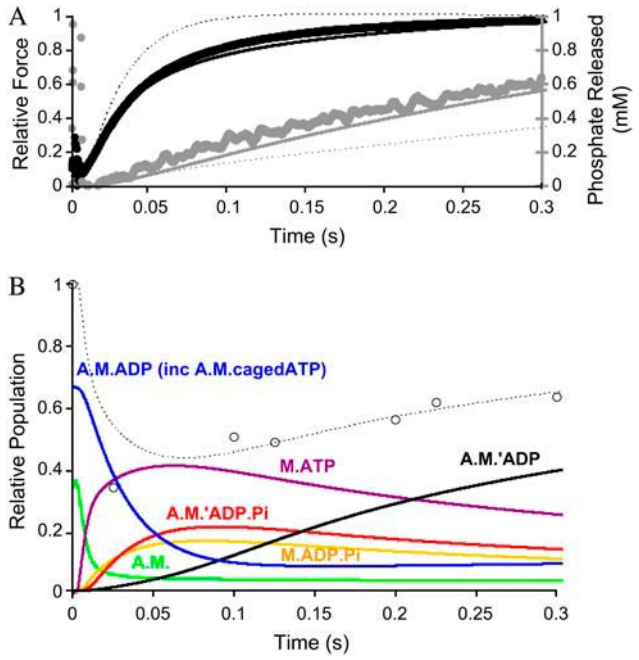

FIGURE 9 Comparison of observed data during the first 0.3 s of activation and the model calculations using Scheme 1 and parameters listed in Table 3. (*A*) Observed (*thick line*) and simulated (*thin lines*) data are the same as shown in Fig. 8 *A* but on an expanded time axis. Tension (*black*) is on the left-hand *y* axis and phosphate release (*gray*) is on the right-hand *y* axis. The calculated tension and phosphate records in the absence of series elasticity (see text) are shown by the dotted lines. (*B*) Relative occupancy of actomyosin states calculated by the model during the first 0.3 s of contraction at 12°C. Actomyosin states are labeled on graph. The A·M·ADP state includes both A·M·ADP (nonforce, ADP bound) and A·M.cagedATP states. The dotted line is the calculated, normalized number of attached cross-bridges. Also shown are the experimentally determined relative changes in fiber stiffness (*open circles*) scaled to relative actomyosin concentrations (see text).

Effect of step size

Imposing rapid length steps on an isometric muscle fiber perturbs the quasi-steady state by relieving strain on stereospecifically bound cross-bridges. The return to the steady state is accompanied by a transient acceleration of the rate of phosphate release, as determined with the MDCC-PBP assay.

The size of the step, and speed with which it is imposed (23), determine the amount of cross-bridge detachment during phases 1 and 2. The bigger step (6 nm hs^{-1}) causes a larger perturbation of the cross-bridges (1), resulting in a larger drop in force and faster phase 2 recovery (1). Experimental data show that the rate at which cross-bridges reequilibrate during phases 3 and 4 (through cross-bridge cycling) is not strain dependent, hence the rates of tension recovery are similar for both 3 and 6 nm hs^{-1} steps at 12°C or 20°C (Table 2). The transient phosphate-release rates are also independent of step size. The amplitude of the phosphate transient provides a direct measurement of the number of force-holding A·M·′ADP·P_i cross-bridges. Larger steps, which perturb more cross-bridges, release more phosphate during the transient. The 6 nm hs^{-1} step caused the release of 52 μM phosphate at 12°C. Assuming a myosin head concentration of 150 μM, this implies 34% of the total cross-bridges are attached and reequilibrate after the step. This estimate falls between previously determined estimates of 20% (25) and 50%, based on x-ray diffraction data (26), of which a temperature-dependent portion would be force generating. The fraction of attached cross-bridges calculated by the model is approximately twice that established from the phosphate transient, though the model accounts for extra attachments resulting from the accumulation of ADP.

In Scheme 1 and in other models (3,11), the steady (isometric) ADP release rate (k_5) from A·M·′ADP is rate limiting and strain dependent. Calculations show that the maximum (unstrained) ADP release rate (xk_5) at 20°C was 3840 s^{-1}, but during initial contraction at the point of maximum rate of tension development, the rate of ADP release is 1500 s^{-1}. Before the step the model predicts A·M·′ADP to be the most populated state (Fig. 9 *B*). In Fig. 10 *A* larger steps, calculated by a reduction in the predicted tension (T_{drop}) to match the drop in experimental tension, cause a greater perturbation in the A·M·′ADP cross-bridge population. The tension drop for a 0.5%*L* step is 1.7 times that of a 0.3%*L* step. The return to the steady state after larger steps requires additional cross-bridge cycling, and hence the amplitude of the phosphate transient is increased.

Effect of temperature

Examination of the rate constants determined by fitting the model to the experimental data shows that temperature enhances various steps in the actomyosin cycle (Table 3). Acceleration of the low strain ADP release rate (xk_5)

speeds cross-bridge detachment, increasing rates of phases 3 and 4 of force redevelopment. Experimentally, the tension recovery rates increase from ~14 s^{-1} at 12°C to ~27 s^{-1} at 20°C.

Isometric tension measured in these experiments is high because MDCC-PBP sequesters the released phosphate, thus preventing it from depressing force (27). Activations in the absence of MDCC-PBP produced tensions ~12% lower (data not shown). Also, isometric tension increases by 28% from 12 to 20°C. It was concluded from temperature jump experiments that individual cross-bridges (A·M·′ADP or A·M·′ADP·P_i) are likely to generate the same force at temperatures between 6°C and 30°C (28). The greater tensions produced at higher temperatures results from an increase in the population of force-generating cross-bridges (26,28). Some of these extra cross-bridges may be due to increased attachments, but this effect was insufficient to account for the large increase in tension (28). Additionally, active stiffness measurements at 12°C and 20°C are similar (here and 28), suggesting similar numbers of cross-bridges are attached. Instead, increased temperature may cause a shift in the distribution of A·M·′ADP·P_i (force) and A·M·ADP·P_i (nonforce) states toward the force-generating form. Such a shift results in an increase in the average cross-bridge force held by the total A·M·′ADP·P_i and A·M·ADP·P_i population at higher temperatures (24,26,28). We have successfully modeled the experimental data with a scheme that includes both force and nonforce A·M·ADP·P_i states (not shown). However there are no data to constrain the rate constants for the transition of A·M·ADP·P_i to A·M·′ADP·P_i. Therefore we present a model where both A·M·ADP.P_i states are grouped together. This state generates force but also accounts for the nonforce A·M·ADP·P_i isoform. As previously stated, the average force assigned to A·M·′ADP·P_i at 12°C is 2 and increases to 3 at 20°C. This is to account for the temperature shift in the A·M·ADP·P_i state distribution.

Experimentally, the transient rate of phosphate release increased from ~33 s^{-1} at 12°C to ~85 s^{-1} at 20°C. These rates, and their temperature dependence (Q_{10} of 3.2), are similar to the fast rate of phosphate release, also measured using the MDCC-PBP probe, for actomyosin in solution (9). The rate of the fast phase (36 s^{-1} at 10°C and 77 s^{-1} at 20°C; Q_{10} of 2.7) relates to the immediate release of phosphate from A·M·ADP·P_i. The similarity of the phosphate transients in isometric fibers and solution agrees with a process that is strain independent. In fibers at 20°C the amplitude of the phosphate transient, for a given step size, decreases by approximately half, indicating a temperature-dependent shift in the distribution of cross-bridge states away from A·M·′ADP·P_i (Scheme 1). This differs from the solution experiments that showed the proportion of total phosphate released from the fast phase was increasing with temperature (9). Calculations show that the reduction is due to an increased buildup of ADP at 20°C, which slows the rate of ADP release. The effects of reduced ADP release rates were seen, experimentally and in the model, in the steady rates of phosphate release which were similar at 12°C and 20°C. In Scheme 1, k_4 (phosphate release) increases with temperature, causing the shift in cross-bridges away from the A·M·′ADP·P_i state. Fig. 10 *A* shows the calculated cross-bridge distributions for A·M·′ADP·P_i and A·M·′ADP states during a step at 12°C and 20°C. At 20°C, there is a greater accumulation of the A·M·′ADP states at the expense of A·M·′ADP·P_i. Accordingly, before a length step at higher temperatures, there are fewer cross-bridges in the A·M·′ADP·P_i state, and so fewer myosin heads are able to release phosphate upon a reduction in strain.

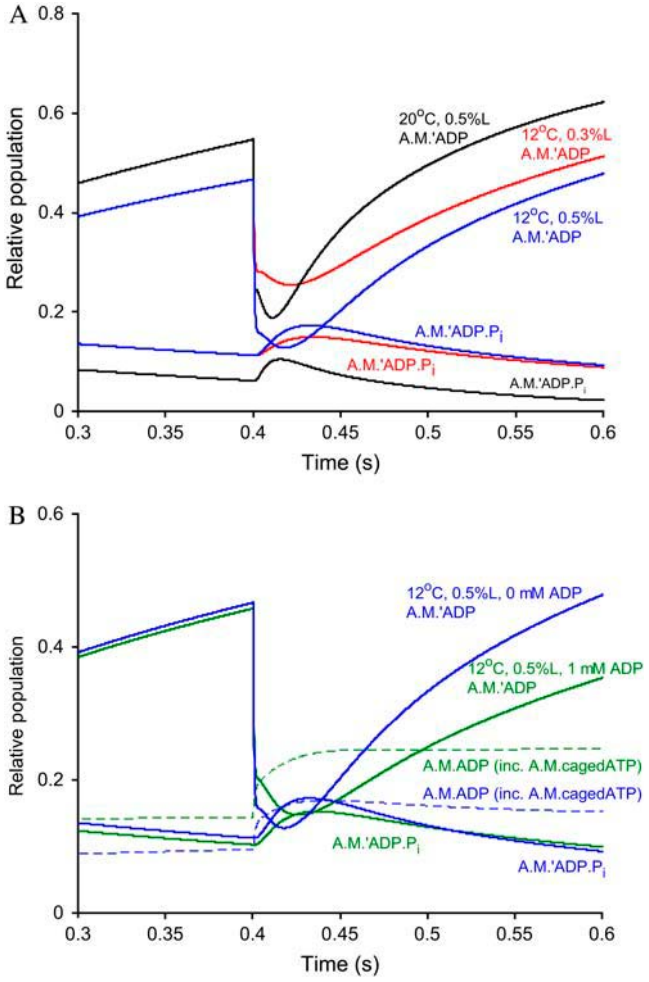

FIGURE 10 Calculated distribution of attached cross-bridges after rapid length steps. (*A*) Relative occupancy of A·M·′ADP·P_i (*thin lines*) and A·M·′ADP (*thick lines*) cross-bridge states during the period of a rapid release step, calculated by the model (Scheme 1) using parameters listed in Table 3. Calculations are shown for 20°C with a 0.5%*L* step (*black*), 12°C with a 0.5%*L* step (*blue*), and 12°C with a 0.3%*L* (*red*). (*B*) Relative occupancy of A·M·′ADP·P_i (*thin lines*), A·M·′ADP (*thick lines*), and A·M·ADP (*dashed lines*) cross-bridge states during the period of a 0.5%*L* step at 12°C with (*green lines*) and without (*blue lines*) 1 mM added ADP. The A·M·ADP state includes both A·M·ADP (nonforce, ADP bound) and A·M.cagedATP states.

Effect of ADP

Length step experiments (0.5%L steps at 12°C) were conducted in the absence and in the presence of either 0.5 or 1.0 mM added ADP. Actomyosin with bound ADP has two states: A·M·′ADP (high force) and A·M·ADP (low/no force), where the former is generated through ATPase cycling (29–31). Scheme 1 was used to model the release step data in the presence of 1 mM added ADP, using the rate constants shown in Table 3 for 12°C. Before NPE-caged ATP photolysis, calculations show that 36% of cross-bridges were A·M·ADP (nonforce, ADP bound) and 45% were A·M.cagedATP. All remaining cross-bridges were in the A·M. state. Experiments show that the rigor tension before activation was unaffected by the presence of ADP (data not shown), being ~20 kN m^{-2}. So A·M·ADP does not generate force, and in the model the A·M·ADP state was introduced as a state external to the actomyosin cycle to avoid a high force to nonforce structural transition before ADP release.

The addition of ADP caused a statistically significant ($p \leq 0.05$, Fig. 7) increase in observed stiffness, suggesting that ADP slows net ADP release in isometric contraction, causing buildup of attached states. Despite the increase in stiffness, the isometric tension was not significantly elevated in the presence of ADP. The presence of MDCC-PBP keeps phosphate low, causing the A·M·′ADP state to be heavily populated. The addition of ADP may not cause further increases in the A·M·′ADP state concentration but causes a buildup of the nonforce A·M·ADP state. This is different to previous reports where 1 mM ADP caused a 10% increase in isometric tension (27,32). In those experiments, however, phosphate built up, possibly increasing A·M·ADP·P_i states (force and nonforce isomers), and hence adding ADP may have caused an increase in force. The calculated time courses of changes in A·M·′ADP·P_i, A·M·′ADP, and A·M·ADP states (where A·M·ADP also includes A·M.cagedATP states) are shown in Fig. 10 *B* for 0 and 1 mM added ADP. Simulations with added ADP had a higher fraction of attached cross-bridges, but there was little effect on the populations of A·M·′ADP·P_i and A·M·′ADP compared to the control (before the step). The extra attachment resulted from an increase in the A·M·ADP population, which does not contribute to the tension. Failure of the fiber to return to the prestep tensions after a quick release is replicated in the calculations. In comparison to the control, recovery of the A·M·′ADP population is slower and incomplete in the presence of added ADP. The poststep reduction in force producing A·M·′ADP states is concurrent with an elevation of the nonforce production A·M·ADP population. The buildup of ADP and A·M·ADP states predicted by the model are responsible for the observed slowing down of phases 3 and 4 of tension recovery after length steps.

Regardless of initial ADP concentration, extra ADP will have accumulated from cross-bridge cycling during contraction. At 0.4 s, based on the MDCC-PBP assay data, ~0.7 mM ADP had been produced in the absence of added ADP. At 0.4 s, with initial ADP concentrations of 0.5 and 1.0 mM, the total ADP was ~1.2 and ~1.7 mM, respectively. Buildup of ADP has been shown to be a factor in reducing ATPase activity (5,11), and added ADP slowed the steady rate of phosphate release, but here the effect was not statistically significant. There was also no significant effect of added ADP on the amount of phosphate released by the step perturbation or the transient rate (Fig. 7). This suggests that, with added ADP, the step causes a similar number of cross-bridges to reequilibrate as in the control. Calculations also show that added ADP does not substantially alter the populations of A·M·′ADP·P_i and A·M·′ADP states (Fig. 10 *B*), and this effect may be particular to the low phosphate environment of these experiments.

CONCLUSION

The experiments performed here reveal the relationship between the strain-dependent transitions in isometric muscle fibers and the phosphate-release step. By relieving strain, through fast and small length steps, ADP release no longer limits the actomyosin ATPase cycle, thus phosphate release (or an associated isomerization) accelerates to rates similar to those seen in solution. The kinetic scheme is able to fit the observed tension and phosphate-release data. Rate constant values for each of the steps in the scheme have been established for 12 and 20°C. Further work is required to incorporate displacement dependence of force-generating cross-bridges in the kinetic model.

Our thanks to M. Webb and J. Hunter for production and supply of the phosphate binding protein, and also M. Webb, J. Corrie, and G. Reid for the MDCC and NPE-caged ATP. We are grateful to D. Trentham and A. Tsaturyan for their helpful comments on the manuscript, and also to J. Sleep, R. Woledge, and N. Curtin for their comments on the kinetic model.

This work is funded by the Medical Research Council (MRC). V.B.S. was supported by an MRC studentship.

REFERENCES

1. Huxley, A. F., and R. M. Simmons. 1971. Proposed mechanism of force generation in striated muscle. *Nature*. 233:533–538.
2. Smith, D. A., and J. Sleep. 2004. Mechanokinetics of rapid tension recovery in muscle: the Myosin working stroke is followed by a slower release of phosphate. *Biophys. J.* 87:442–456.
3. Sleep, J., M. Irving, and K. Burton. 2005. The ATP hydrolysis and phosphate release steps control the time course of force development in rabbit skeletal muscle. *J. Physiol.* 563:671–687.
4. Brune, M., J. L. Hunter, J. E. Corrie, and M. R. Webb. 1994. Direct, real-time measurement of rapid inorganic phosphate release using a novel fluorescent probe and its application to actomyosin subfragment 1 ATPase. *Biochemistry*. 33:8262–8271.
5. He, Z. H., R. K. Chillingworth, M. Brune, J. E. Corrie, D. R. Trentham, M. R. Webb, and M. A. Ferenczi. 1997. ATPase kinetics on activation

of rabbit and frog permeabilized isometric muscle fibres: a real time phosphate assay. *J. Physiol.* 501:125–148.

6. He, Z. H., R. K. Chillingworth, and M. A. Ferenczi. 1998. The ATPase activity in isometric and shortening skeletal muscle fibres. *Adv. Exp. Med. Biol.* 453:331–341.
7. He, Z. H., R. K. Chillingworth, M. Brune, J. E. Corrie, M. R. Webb, and M. A. Ferenczi. 1999. The efficiency of contraction in rabbit skeletal muscle fibres, determined from the rate of release of inorganic phosphate. *J. Physiol.* 517:839–854.
8. Lionne, C., B. Iorga, R. Candau, N. Piroddi, M. R. Webb, A. Belus, F. Travers, and T. Barman. 2002. Evidence that phosphate release is the rate-limiting step on the overall ATPase of psoas myofibrils prevented from shortening by chemical cross-linking. *Biochemistry.* 41:13297–13308.
9. White, H. D., B. Belknap, and M. R. Webb. 1997. Kinetics of nucleoside triphosphate cleavage and phosphate release steps by associated rabbit skeletal actomyosin, measured using a novel fluorescent probe for phosphate. *Biochemistry.* 36:11828–11836.
10. Hibberd, M. G., and D. R. Trentham. 1986. Relationships between chemical and mechanical events during muscular contraction. *Annu. Rev. Biophys. Biophys. Chem.* 15:119–161.
11. West, T. G., N. A. Curtin, M. A. Ferenczi, Z. H. He, Y. B. Sun, M. Irving, and R. C. Woledge. 2004. Actomyosin energy turnover declines while force remains constant during isometric muscle contraction. *J. Physiol.* 555:27–43.
12. Thirlwell, H., J. E. Corrie, G. P. Reid, D. R. Trentham, and M. A. Ferenczi. 1994. Kinetics of relaxation from rigor of permeabilized fast-twitch skeletal fibers from the rabbit using a novel caged ATP and apyrase. *Biophys. J.* 67:2436–2447.
13. He, Z., G. J. Stienen, J. P. Barends, and M. A. Ferenczi. 1998. Rate of phosphate release after photoliberation of adenosine 5′-triphosphate in slow and fast skeletal muscle fibers. *Biophys. J.* 75:2389–2401.
14. Brune, M., J. L. Hunter, S. A. Howell, S. R. Martin, T. L. Hazlett, J. E. Corrie, and M. R. Webb. 1998. Mechanism of inorganic phosphate interaction with phosphate binding protein from Escherichia coli. *Biochemistry.* 37:10370–10380.
15. Dantzig, J. A., Y. E. Goldman, N. C. Millar, J. Lacktis, and E. Homsher. 1992. Reversal of the cross-bridge force-generating transition by photogeneration of phosphate in rabbit psoas muscle fibres. *J. Physiol.* 451:247–278.
16. Ford, L. E., A. F. Huxley, and R. M. Simmons. 1977. Tension responses to sudden length change in stimulated frog muscle fibres near slack length. *J. Physiol.* 269:441–515.
17. Urbanke, C., and J. Wray. 2001. A fluorescence temperature-jump study of conformational transitions in myosin subfragment 1. *Biochem. J.* 358:165–173.
18. Thirlwell, H., J. A. Sleep, and M. A. Ferenczi. 1995. Inhibition of unloaded shortening velocity in permeabilized muscle fibres by caged ATP compounds. *J. Muscle Res. Cell Motil.* 16:131–137.
19. Tsaturyan, A. K., N. Koubassova, M. A. Ferenczi, T. Narayanan, M. Roessle, and S. Y. Bershitsky. 2005. Strong binding of myosin heads stretches and twists the actin helix. *Biophys. J.* 88:1902–1910.
20. Smith, N. P., C. J. Barclay, and D. S. Loiselle. 2005. The efficiency of muscle contraction. *Prog. Biophys. Mol. Biol.* 88:1–58.
21. Goldman, Y. E., M. G. Hibberd, and D. R. Trentham. 1984. Initiation of active contraction by photogeneration of adenosine-5′-triphosphate in rabbit psoas muscle fibres. *J. Physiol.* 354:605–624.
22. Hilber, K., Y. B. Sun, and M. Irving. 2001. Effects of sarcomere length and temperature on the rate of ATP utilisation by rabbit psoas muscle fibres. *J. Physiol.* 531:771–780.
23. Lombardi, V., G. Piazzesi, and M. Linari. 1992. Rapid regeneration of the actin-myosin power stroke in contracting muscle. *Nature.* 355: 638–641.
24. Piazzesi, G., M. Reconditi, N. Koubassova, V. Decostre, M. Linari, L. Lucii, and V. Lombardi. 2003. Temperature dependence of the force-generating process in single fibres from frog skeletal muscle. *J. Physiol.* 549:93–106.
25. Cooke, R., M. S. Crowder, and D. D. Thomas. 1982. Orientation of spin labels attached to cross-bridges in contracting muscle fibres. *Nature.* 300:776–778.
26. Ferenczi, M. A., S. Y. Bershitsky, N. Koubassova, V. Siththanandan, W. I. Helsby, P. Panine, M. Roessle, T. Narayanan, and A. K. Tsaturyan. 2005. The ''roll and lock'' mechanism of force generation in muscle. *Structure.* 13:131–141.
27. Cooke, R., and E. Pate. 1985. The effects of ADP and phosphate on the contraction of muscle fibers. *Biophys. J.* 48:789–798.
28. Bershitsky, S. Y., and A. K. Tsaturyan. 2002. The elementary force generation process probed by temperature and length perturbations in muscle fibres from the rabbit. *J. Physiol.* 540:971–988.
29. Dantzig, J. A., M. G. Hibberd, D. R. Trentham, and Y. E. Goldman. 1991. Cross-bridge kinetics in the presence of MgADP investigated by photolysis of caged ATP in rabbit psoas muscle fibres. *J. Physiol.* 432:639–680.
30. Sleep, J. A., and R. L. Hutton. 1980. Exchange between inorganic phosphate and adenosine 5′-triphosphate in the medium by actomyosin subfragment 1. *Biochemistry.* 19:1276–1283.
31. Horiuti, K., N. Yagi, and S. Takemori. 1997. Mechanical study of rat soleus muscle using caged ATP and x-ray diffraction: high ADP affinity of slow cross-bridges. *J. Physiol.* 502:433–447.
32. Wang, G., and M. Kawai. 1996. Effects of MgATP and MgADP on the cross-bridge kinetics of rabbit soleus slow-twitch muscle fibers. *Biophys. J.* 71:1450–1461.